PERGAMON

International Journal of Heat and Mass Transfer 44 (2001) 4625–4633

International Journal of HEAT and MASS TRANSFER

www.elsevier.com/locate/ijhmt

Stability analysis of double-diffusive convection in superposed fluid and porous layers using a one-equation model

Pinghua Zhao, C.F. Chen *

Department of Aerospace and Mechanical Engineering, The University of Arizona, Aero Building #16, Tucson, AZ 85721, USA

Received 16 October 2000; received in revised form 8 March 2001

Abstract

Linear stability analysis has been carried out to predict the onset of double-diffusive convection in superposed fluid and porous layers using a one-equation model. The eigenvalue problem is solved numerically by a finite difference scheme. Results have been obtained for the thermal convection and salt-finger cases. Comparing with the results obtained for the same problems by Chen and Chen [F. Chen, C.F. Chen, J. Heat Transfer 110 (1988) 403–409] using a two-equation model, we find that these two methods give the same general characteristics of the marginal stability curves, however, there are differences in the critical conditions and the flow streamlines at onset. Carefully conducted experiments are needed to determine which model gives the more realistic results.

Keywords: Stability analysis; Superposed layers; One-equation model

1. Introduction

When a binary alloy is directionally solidified by cooling from below, a mushy layer consisting of a solid matrix of dendritic crystals saturated with liquid melt is sandwiched between a liquid layer above and a solid layer below as show in Fig. 1(a). A typical temperature (T) and concentration (C) distribution within liquid and mushy layers is sketched in Fig. 1(b) for Pb–Sb (2.2 wt%) solidifying at a low rate ($\sim\mu$m/s). Since Sb is much lighter than Pb, the larger concentration of Sb on the bottom means lower density there. The solutal concentration distribution is destabilizing while the temperature distribution is stabilizing. Double-diffusive convection is generated which eventually leads to plume convection and chimney formation in the mushy zone resulting in a defective casting, see for example, experiments of Sample and Hellawell [1], Chen and Chen [2] and Tait and Jaupart [3]. Linear stability and weakly non-linear analysis of the problem have been carried out by Worster [4], Chen et al. [5], Anderson and Worster [6] and Chung and Chen [7], among others. Such analyses were made with a two-equation model of the fluid motion, i.e., one set of conservation equations each governing the fluid motion in the liquid and in the mushy layers which are coupled by a set of suitable boundary conditions at the interfacial region. A detailed summary of the method of analysis and the results obtained are given by Worster [8] in a recent review article.

In the same time period, a number of numerical simulations of the directional solidification process have been carried out using a one-equation model to describe the fluid motion in both the liquid and the mushy layers. See, for example, [9–13]. In this formulation, the porosity ϕ (which assumes the value 0 in the solid, $0 < \phi < 1$ within mush, and 1 in the liquid) is the marker parameter which locates the point under consideration into the correct region. In this manner, the solidification problem becomes less complicated than those based on the two-equation model, and at the same time yields results which are reasonable as compared to those obtained from experiments. Nandapurkar et al. [14] used the one-equation model to consider the linear

* Corresponding author. Tel.: +1-520-621-8199; fax: +1-520-621-8191.

E-mail address: chen@ame.arizona.edu (C.F. Chen).

0017-9310/01/$ - see front matter
PII: S0017-9310(01)00102-8

Nomenclature

a	non-dimensional wave number, $a = kd$
b_T	basic temperature gradient, dT_B/dz
b_C	basic concentration gradient, dC_B/dz
C, C_0, C_B	solutal concentration, sub '0' indicates reference, 'B' basic state
d	thickness of domain, $d = d_l + d_p$
d_l, d_p	thickness of fluid and porous layers
$\hat{d}$	depth ratio $= d_l/d_p$
g	gravity constant
k	dimensional wave number
K	permeability, a function of porosity φ
K_0	reference permeability
P	pressure
R_a, R_C	thermal and solutal Rayleigh numbers
T, T_0, T_B	temperature, sub '0' indicates reference, 'B' basic state
t	time
u, w	velocity components in x and z directions
W	normalized non-dimensional vertical velocity

Greek symbols

α_T, α_C	thermal and mass diffusivities
α_{Tl}, α_{Tp}	thermal diffusivity of fluid and porous layers
α_{Cl}, α_{Cp}	mass diffusivity of fluid and porous layers
β_T, β_C	thermal and solutal expansion coefficients
δ	Darcy number $= \sqrt{K}/d_m$
ϕ	porosity
$\varepsilon_T, \varepsilon_C$	$\alpha_{Tl}/\alpha_{Tp}, \alpha_{Cl}/\alpha_{Cp}$
ρ, ρ_0	density and reference density
v_0	kinematic viscosity

Subscripts

0	reference
l, p	liquid and porous layers
B	basic state
T, C	temperature and concentration

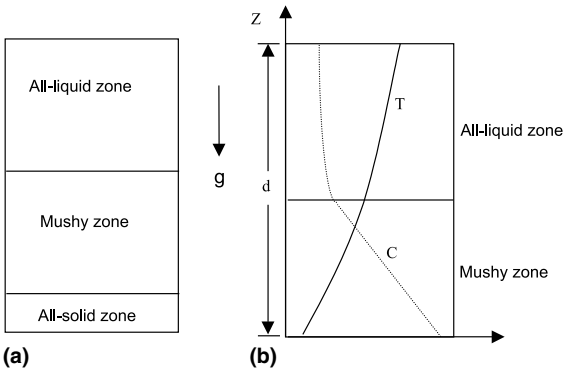

Fig. 1. (a) Three zones in directional solidification. (b) Temperature and solutal concentration distributions when the mushy zone has just fully developed (no all-solid zone at this moment).

stability of a Pb–20 wt% Sn alloy under directional solidification. Their results are obtained for a given freezing speed and are in dimensional terms.

The question arises whether a stability analysis based on the one-equation model will yield comparable results as those obtained with the two-equation model. To answer this question, we have performed linear stability analysis using the one-equation model on the thermal–solutal convection in superposed liquid and porous layers, and the results are compared to those of Chen and Chen [15] who have performed linear stability analysis of the same problem using the two-equation model. In the present problem, no freezing or remelting is considered in the porous layer. In the following, the equations are derived in Section 2, the method of solution is presented in Section 3, and the results and discussion are presented in Section 4 followed by conclusions.

2. Equations

Consider a fluid layer of thickness d_l overlaying a porous layer of thickness d_p with a total thickness $d = d_l + d_p$. The porosity of the porous layer is ϕ which may be a function of vertical coordinate z. The density of fluid is assumed to be linear in T and C:

$$\rho = \rho_0[1 - \beta_T(T - T_0) - \beta_C(C - C_0)],$$

where $\beta_T = -(1/\rho)(\partial\rho/\partial T)$ is the thermal expansion coefficient and $\beta_C = -(1/\rho)(\partial\rho/\partial C)$ is the expansion coefficient due to solute concentration.

The two-dimensional continuity, momentum, energy and solutal concentration equations for a Boussinesq substance valid for either the fluid or the porous layer are [14]:

$$\frac{\partial u}{\partial x} + \frac{\partial w}{\partial z} = 0, \tag{1}$$

$$\phi\frac{\partial}{\partial t}\left(\frac{u}{\phi}\right) + u\frac{\partial}{\partial x}\left(\frac{u}{\phi}\right) + w\frac{\partial}{\partial z}\left(\frac{u}{\phi}\right) = -\frac{\phi}{\rho_0}\frac{\partial p}{\partial x} - \frac{v_0\phi}{K_X}u + v_0\nabla^2 u, \tag{2}$$

$$\phi\frac{\partial}{\partial t}\left(\frac{w}{\phi}\right)+u\frac{\partial}{\partial x}\left(\frac{w}{\phi}\right)+w\frac{\partial}{\partial z}\left(\frac{w}{\phi}\right)$$
$$=-\frac{\phi}{\rho_0}\frac{\partial p}{\partial z}-\frac{v_0\phi}{K_Z}w+v_0\nabla^2 w-\frac{\phi g}{\rho_0}\rho, \tag{3}$$

$$\frac{\partial T}{\partial t}+u\frac{\partial T}{\partial x}+w\frac{\partial T}{\partial z}=\alpha_{\mathrm{T}}\left(\frac{\partial^2 T}{\partial x^2}+\frac{\partial^2 T}{\partial z^2}\right), \tag{4}$$

$$\phi\frac{\partial C}{\partial t}+u\frac{\partial C}{\partial x}+w\frac{\partial C}{\partial z}$$
$$=\alpha_{\mathrm{C}}\left[\frac{\partial}{\partial x}\left(\phi\frac{\partial C}{\partial x}\right)+\frac{\partial}{\partial z}\left(\phi\frac{\partial C}{\partial z}\right)\right], \tag{5}$$

where $\alpha_{\mathrm{T}}=\alpha_{\mathrm{Tl}}$, $\alpha_{\mathrm{C}}=\alpha_{\mathrm{Cl}}$ in the liquid layer and $\alpha_{\mathrm{T}}=\alpha_{\mathrm{Tp}}$, $\alpha_{\mathrm{C}}=\alpha_{\mathrm{Cp}}$ in the porous layer. Since no freezing or re-melting is considered in the porous layer, there is no latent heat term in Eq. (4).

The conditions at the top and bottom boundaries are zero velocity with given values of T and C. The basic state is quiescent and we seek the critical conditions when fluid motion onsets.

The linearized perturbation equations are:

$$\frac{\partial u'}{\partial x}+\frac{\partial w'}{\partial z}=0, \tag{6}$$

$$\frac{\partial u'}{\partial t}=-\frac{\phi}{\rho_0}\frac{\partial P'}{\partial x}-\frac{v_0\phi}{K_X}u'+v_0\nabla^2 u', \tag{7}$$

$$\frac{\partial w'}{\partial t}=-\frac{\phi}{\rho_0}\frac{\partial P'}{\partial z}-\frac{v_0\phi}{K_Z}w'+v_0\nabla^2 w'$$
$$+\phi g(\beta_{\mathrm{T}}T'+\beta_{\mathrm{C}}C'), \tag{8}$$

$$\frac{\partial T'}{\partial t}=\alpha_{\mathrm{T}}\nabla^2 T'-b_{\mathrm{T}}w', \tag{9}$$

$$\frac{\partial C'}{\partial t}=\alpha_{\mathrm{C}}\nabla^2 C'-\frac{b_{\mathrm{C}}}{\phi}w'+\frac{\alpha_{\mathrm{C}}}{\phi}\frac{\mathrm{d}\phi}{\mathrm{d}z}\frac{\partial C'}{\partial z}, \tag{10}$$

where the prime denotes perturbation, and $b_{\mathrm{T}}=\mathrm{d}T_{\mathrm{B}}/\mathrm{d}z$ and $b_{\mathrm{C}}=\mathrm{d}C_{\mathrm{B}}/\mathrm{d}z$ are temperature and concentration gradients at the basic state. Normally b_{T} is set to be constant but b_{C} may not be. When porosity is constant in porous layer, b_{C} is constant but may be different in different layers.

Applying normal mode analysis, we assume

$$w'=W(z)\,\mathrm{e}^{\mathrm{i}kx+pt},$$
$$T'=T(z)\,\mathrm{e}^{\mathrm{i}kx+pt},$$
$$C'=C(z)\,\mathrm{e}^{\mathrm{i}kx+pt}.$$

When these are substituted into Eqs. (6)–(10) with the elimination of the pressure and assuming steady onset into steady convection ($p=0$), we obtain

$$\frac{1}{\phi}(D^2-k^2)^2W-\left(\frac{1}{\phi^2}\frac{\mathrm{d}\phi}{\mathrm{d}z}\right)D(D^2-k^2)W$$
$$+\frac{1}{K_Z}k^2W-\frac{1}{K_X}D^2W-\frac{\mathrm{d}}{\mathrm{d}z}\left(\frac{1}{K_X}\right)DW$$
$$-\frac{g\beta_{\mathrm{T}}k^2}{v_0}T-\frac{g\beta_{\mathrm{C}}k^2}{v_0}C=0, \tag{11}$$

$$(D^2-k^2)T=\frac{b_r}{\alpha_{\mathrm{T}}}W, \tag{12}$$

$$\left(D^2+\frac{1}{\phi}\frac{\mathrm{d}\phi}{\mathrm{d}z}D-k^2\right)C=\frac{b_{\mathrm{C}}}{\phi\alpha_{\mathrm{C}}}W, \tag{13}$$

where $D=\mathrm{d}/\mathrm{d}z$ (differential operator). When these equations are non-dimensionalized with respect to characteristic length d, velocity α_{Tl}/d, $\Delta T=T_2-T_1$, and $\Delta C=C_2-C_1$, where subscripts '2' and '1' denote the top and bottom boundaries respectively, we finally obtain the following linear stability equations:

$$\frac{K_0}{\phi}(D^2-a^2)^2W-\left(\frac{K_0}{\phi^2}\frac{\mathrm{d}\phi}{\mathrm{d}z}\right)D(D^2-a^2)W$$
$$+a^2\frac{K_0}{K_Z}W-\frac{K_0}{K_X}D^2W-\frac{\mathrm{d}}{\mathrm{d}z}\left(\frac{K_0}{K_X}\right)DW$$
$$-a^2R_{\mathrm{a}}T-a^2R_{\mathrm{C}}C=0, \tag{14}$$

$$(D^2-a^2)T=\frac{\alpha_{\mathrm{Tl}}}{\alpha_{\mathrm{T}}}W, \tag{15}$$

$$\left(D^2+\frac{1}{\phi}\frac{\mathrm{d}\phi}{\mathrm{d}z}D-a^2\right)C=\frac{1}{\phi}\left(\frac{b_{\mathrm{C}}d}{\Delta C}\right)\left(\frac{\alpha_{\mathrm{Cl}}}{\alpha_{\mathrm{C}}}\right)W, \tag{16}$$

where the temperature and concentration Rayleigh numbers are

$$R_{\mathrm{a}}=\frac{g\beta_{\mathrm{T}}\Delta TK_0d^3}{v_0\alpha_{\mathrm{Tl}}},\quad R_{\mathrm{C}}=\frac{g\beta_{\mathrm{C}}\Delta CK_0d^3}{v_0\alpha_{\mathrm{Cl}}}$$

and the wave number $a=kd$. In these equations, K_0 is a suitable non-dimensional constant to scale down the equation because K is usually very small. The choice of K_0 is arbitrary. It can be $K(\phi=0.5)$, for instance.

The boundary conditions are

$$W=T=C=DW=0\quad\text{at } z=0 \text{ and } 1.$$

3. Method of solution

For any given porosity distribution $\phi(z)$ and corresponding permeability $K(z)$, the system of equations (14)–(16) plus the boundary conditions is an eigenvalue problem for a, R_{a} and R_{C}. Our goal is to find the relationship between these three variables which makes the problem have non-trivial solutions for W, T and C. The method of solution is the following.

The fluid layer is divided into m sub-layers with $(m+1)$ nodes (from 0 to m), Fig. 2. Finite difference method with second-order accurate discretizations is used to transform the differential equations into a system of difference equations, in matrix form, $AX=0$, where A is a $3(m-1)$ by $3(m-1)$ matrix which contains $a, R_{\mathrm{a}}, R_{\mathrm{C}}$ and

$$X=[W_1,T_1,C_1,W_2,T_2,C_2,\ldots\ldots,W_{m-1},T_{m-1},C_{m-1}]^{\mathrm{T}}$$

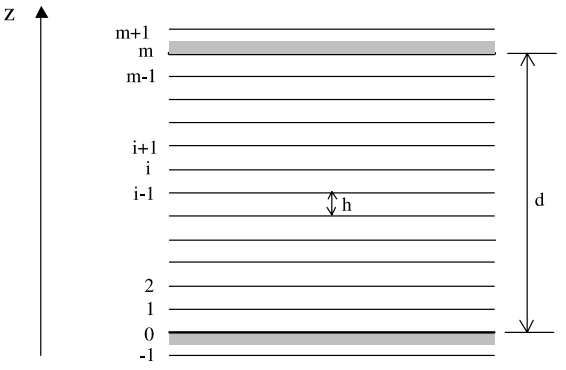

Fig. 2. Discretization: uniform grid in z direction, $h = d/m$, d is the thickness of the whole layer, h is the sub-layer thickness, m is the number of sub-layers.

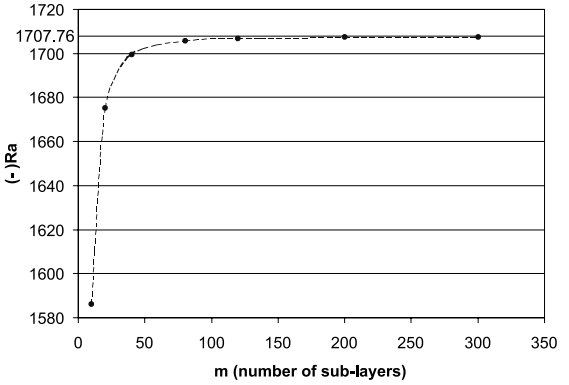

Fig. 3. Grid dependence test for Rayleigh–Benard problem. (–) R_a is the critical Rayleigh number at critical wave number $a = 3.117$. The dashed line is the numerical result for different grids. The solid line indicates the theoretical results.

is the vector containing the values of W, T, and C in the inner nodal points.

In order to have non-trivial solutions for X (i.e., W, T, C), the determinant of A must be zero, namely $\det(A) = 0$, which gives the following relation:

$$f(a, R_a, R_C) = 0.$$

The procedure to solve $f(a, R_a, R_C) = 0$ for critical a, R_a and R_C is the following.

(0) Set a value for R_C (or R_a) depending on the problem considered.
(1) Choose a starting value for a.
(2) For a sufficiently large range of R_a (or R_C), search for the smallest R_a (or R_C) that makes $\det(A) = 0$. This gives a set of data $[a, R_a, R_C]$.
(3) Change a by a given step size. Repeat step (2).
(4) Repeat step (3) for a sufficiently large range of a until a minimum R_a (or R_C) is found (if there exists one). This minimum is the critical Rayleigh number and the corresponding a is the critical wave number.
(5) For this set of critical values $[a, R_a, R_C]$, calculate the eigenvalues and eigenvectors of matrix A. Extract the velocity component (W) from the eigenvectors and calculate the streamfunctions.

4. Results and discussion

4.1. Preliminary calculations

A set of preliminary calculations has been made to validate the method of analysis and the numerical code. For this purpose, we used the present method to obtain the critical condition for the Rayleigh–Benard problem by setting $\phi = 1$, $R_C = 0$, $1/K = 0$ and $K_0 = 1$. With the number of nodes $m = 200$, we obtain the critical $R_a = 1706$ and wave number $a = 3.12$ as compared to the exact values $R_a = 1707$ and $a = 3.117$ with an error of 0.1%. We also used the Rayleigh–Benard problem to test the number of nodes needed to obtain accurate solutions. The results as shown in Fig. 3 indicate very fast convergence to the exact solution [16]. In all subsequent calculations, m is set to 200.

To test the method for a porous layer we consider the Rayleigh–Benard problem for such a layer with $\phi = 0.39$, $R_C = 0$, $1/K = 1.344 \times 10^9$ (any constant $> 10^6$) and $K_0 = K$. The results are $R_a = 39.458$ and $a = 3.14$ which agrees well with the exact solution [17].

4.2. Onset of thermal convection in superposed fluid and porous layers

Chen and Chen [15] have considered this problem using a two-equation model. In order to compare with their results, we set the following variables in terms of the depth ratio $\hat{d}$ and the Darcy number δ which is set to be 0.003 (note the non-dimensional thickness of the whole layer is unity):

$$d_l = \frac{1}{1+\hat{d}}, \quad d_m = \frac{\hat{d}}{1+\hat{d}}, \quad \frac{1}{K} = \frac{(1+\hat{d})^2}{\delta^2}, \quad K_0 = K. \tag{17}$$

The marginal stability curves for different depth ratios are presented in Fig. 4 in which the critical Rayleigh number is shown as a function of the wave number a. Similar to the results of Chen and Chen [15], we found the marginal stability curve is bimodal at low depth ratios. When the depth ratio is smaller than the critical, the long-wave branch is the most critical, whereas when the depth ratio is greater than the critical, the short-wave branch is the most critical. In our case, we found the critical depth ratio is approximately 0.095 while Chen and Chen [15] found the critical value to be 0.13. The reason for this discrepancy is the different nature of the

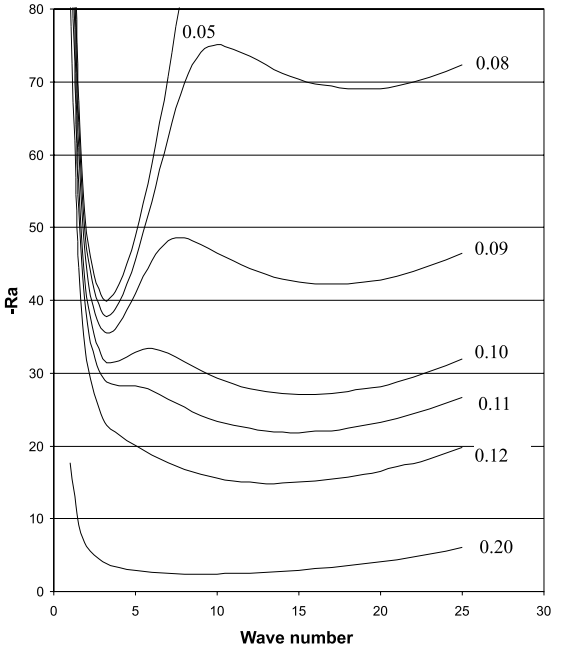

Fig. 4. Marginal stability curves for the thermal convection case. The numbers denote depth ratios.

interfacial conditions imposed in the model equations used. However, the essential bimodal characteristics of the instability are captured by both solutions.

The variations of the critical wave number and the Rayleigh number with the depth ratio are shown in Figs. 5(a) and (b), respectively, together with the results from Fig. 2 in [15]. Since the definitions of the Rayleigh number and wave number are different in the two models, we have converted their data to conform to our definitions. While Chen and Chen [15] used interface and bottom temperatures and the thickness of the porous layer in their definition of the Rayleigh number, it is natural and convenient for a one-equation model to use top and bottom temperature and the thickness of the whole layer. The conversions between the two models are

$$R_a = R_{a_m}\left(\frac{\varepsilon_T + \hat{d}}{\varepsilon_T^2}\right)(1+\hat{d}) \tag{18}$$

and

$$a = a_m(1+\hat{d}), \tag{19}$$

where R_{a_m} and a_m were used in [15].

For the one-equation model, the critical wave number remains essentially constant at the value for a porous layer up to the critical depth ratio of 0.095, Fig. 5(a), then it increases approximately five-fold precipitously when the short-wave mode became the critical instability. As the depth ratio increases, the critical wave number relaxes back almost to its initial value when the depth ratio reaches 1. This trend agrees well with that of Chen and Chen [15], but the values are 30–40% different with the one-equation model giving smaller values. For the critical Rayleigh number, Fig. 5(b), both the trend and the value agree well for the two models. The Rayleigh number starts at $4\pi^2/\varepsilon_T$ ($\varepsilon_T = 0.7$) when depth ratio is zero and decreases with depth ratio continuously until it approaches zero at a depth ratio of 0.5. Results of both models show a change of slope at their respective critical wave number, which is 0.095 for the one-equation model and 0.13 for Chen and Chen's model [15].

In Fig. 6, we present the streamline patterns within one wavelength of the instability flow at onset for depth ratios 0.05–1.0. In these figures, the horizontal lines indicate the liquid–porous interface. For depth ratios up to 0.08, Fig. 6(a), the streamline patterns are essentially the same as those for a porous layer. The effect of the thin liquid layer above is quite minimal. But for $\hat{d} = 0.1$ Fig. 6(b), exceeding the critical depth ratio, the convection is confined mainly within the liquid layer with some motion in the upper region of the porous layer. As

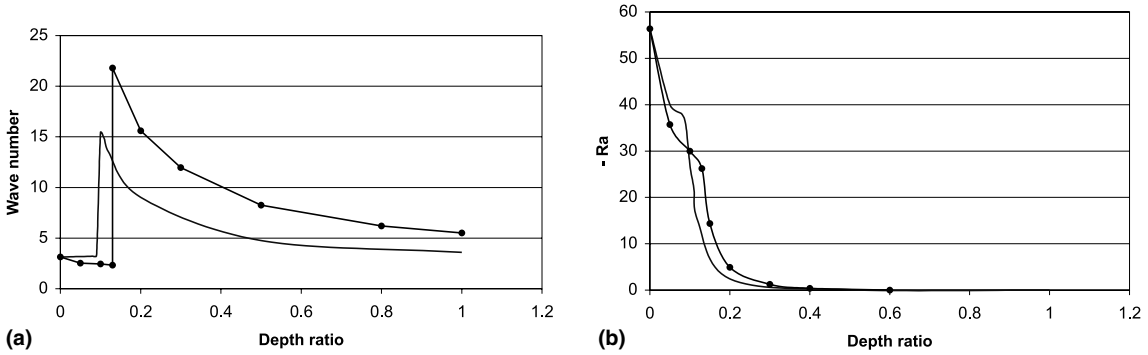

Fig. 5. Critical wave number and Rayleigh number versus depth ratio for the thermal convection case. (a) Wave number, and (b) Rayleigh number. Lines with dots are results converted from [15].

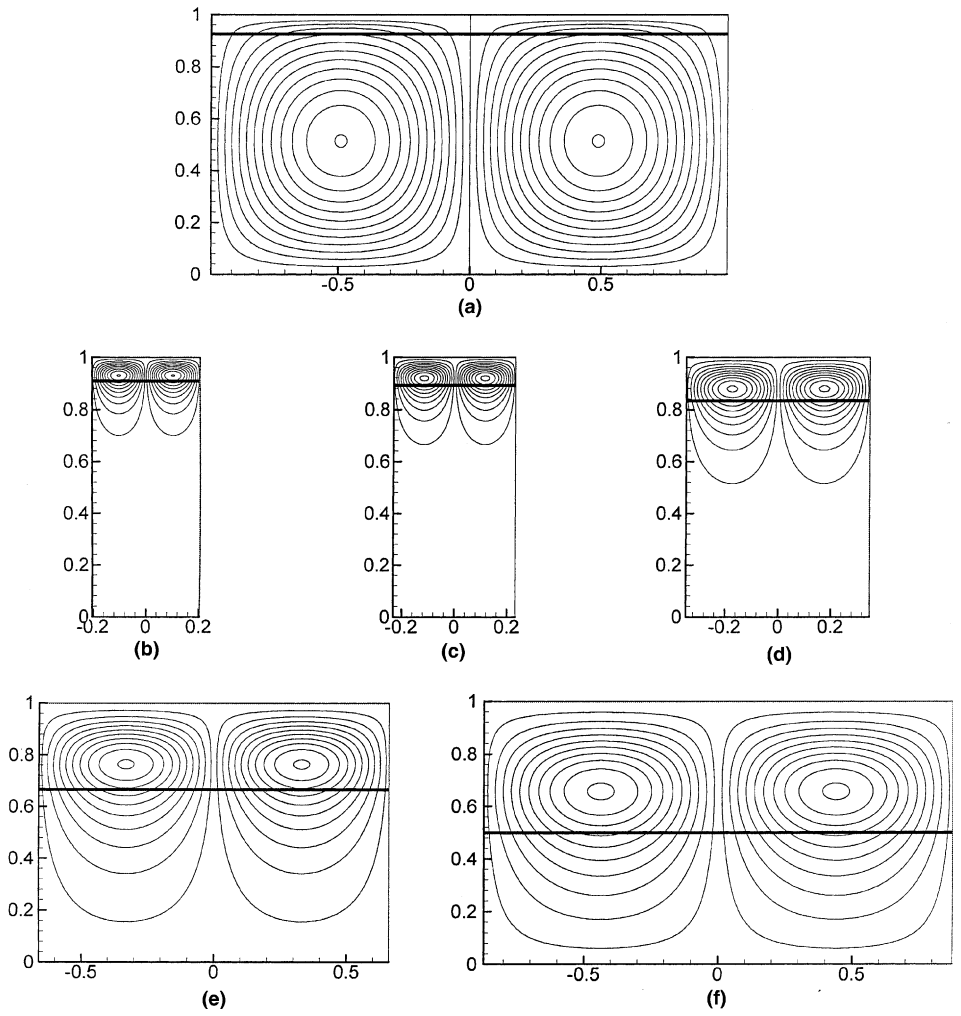

Fig. 6. Streamline patterns at onset for the thermal convection case. The thick horizontal lines denote the liquid–porous interfaces. Depth ratios: (a) 0.08; (b) 0.1; (c) 0.12; (d) 0.2; (e) 0.5; (f) 1.0.

the depth ratio increases, convection penetrates deeper and deeper, Figs. 6(c)–(e), and the wavelengths of the convection cells become larger. At $\hat{d} = 1.0$, Fig. 6(f), fluid motion is found in the entire porous layer. When these figures are compared with those of Chen and Chen [15], the two-equation model presents a much stiffer interface through which the motion in the fluid layer is greatly damped.

For the thermal convection case, the one-equation model captures the essential characteristics of the instability as presented by the two-equation model. However, there are differences in the critical values as shown in Figs. 5(a) and (b). Chen and Chen [18] conducted experiments with a water layer overlaying a porous layer of glass beads in a tank with an aspect ratio (length/width) of 2. Onset of convection was determined by heat flux measurement. The convection pattern was determined by visualization of the temperature distribution on the top surface of the water layer using a liquid crystal film. The experimentally determined critical Rayleigh numbers at six depth ratios, $\hat{d} = 0$, 0.025, 0.1, 0.2, 0.5 and 1.0 agreed very well with the prediction of Chen and Chen [15], see [18, Fig. 1]. Since the present results of the critical Rayleigh number agree well with those of [15] as shown in Fig. 5(b), we have confidence in the one-equation model to predict such critical values. We note here that heat flux measurements at supercritical Rayleigh numbers reported in [18] agreed well with the non-linear computations carried out in [19].

The experiments of Chen and Chen [18] showed that the convection pattern was three-dimensional. The average wave numbers of these convection plumes at the same six depth ratios were compared to the prediction of [15]. The agreement was good at depth ratios lower

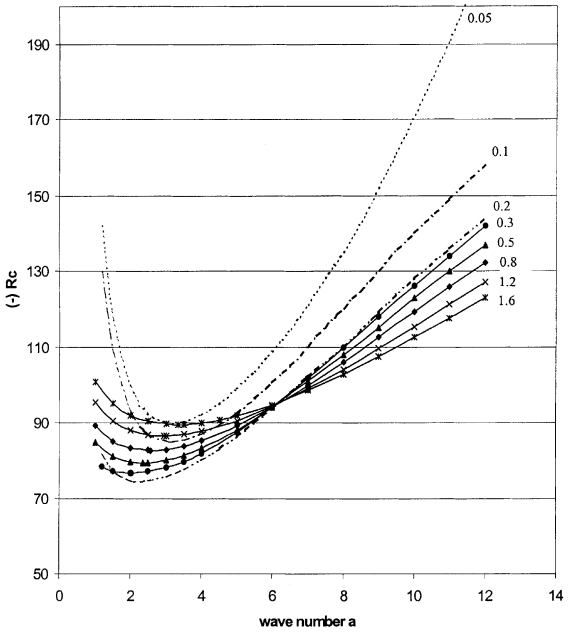

Fig. 7. Marginal stability curves for the salt-finger case. The numbers besides the curves denote the depth ratios.

than the critical value. For depth ratio greater than the critical, the experimental errors became very large and the comparison was not as satisfactory. The present results show that the one-equation model predicts lower critical depth ratio and critical wave numbers than those predicted by the two-equation model. It is possible then to determine which model is the more realistic one by carrying out careful experiments to measure the wave number. In order to do this, the experiment must be carried out at larger aspect ratios so that the instability will be two-dimensional. Secondly, modern techniques such as MRI or CT scan should be used to determine more precisely the size of the convection cells. And careful experiments should be carried out in the depth ratio range of $0.095 \leqslant \hat{d} \leqslant 0.13$ to determine the critical depth ratio. With these results at hand, meaningful comparison can be make about these two models.

4.3. Onset of salt-finger convection in superposed fluid and porous layers

In order to compare our results with Chen and Chen [15], the same parameter values are used:

$$R_a = 50, \quad \delta = 0.003, \quad \varepsilon_T = 0.7, \quad \varepsilon_S = 3.75.$$

As in the thermal convection case, we first show the marginal stability curves for depth ratios from 0.05 to 1.6 in Fig. 7. Within the wave numbers considered up to $a = 14$, no bimodal characteristics of the instability is evident. Chen and Chen [15] did find bimodal behavior at higher wave numbers but the short-wave branch never became the critical one. When the depth ratio is increased from 0.05 to 0.2, the critical solutal Rayleigh number decreases as well as the critical wave number. Beyond $\hat{d} = 0.2$, the system becomes more stable as the depth ratio is increased. This reversal was also found by Chen and Chen [15], although it occurred at a smaller depth ratio.

The variations of the critical wave number and solutal Rayleigh number with depth ratio are presented in Fig. 8. Both the critical wave number and the solutal Rayleigh number decrease sharply at first, reaching their respective minimum values, then increase gradually as the depth ratio is increased from 0.3 to 1.6. The wave number reaches its minimum at $\hat{d} = 0.3$, whereas the solutal Rayleigh number reaches its minimum at $\hat{d} \approx 0.2$. The behavior of these critical characteristics is different from the results of Chen and Chen [15]. Their results show that after attaining the minimum, both the wave number and the Rayleigh number increase to constant values as for $\hat{d} \geqslant 0.4$.

The streamline patterns at onset of instability are shown in Fig. 9 for increasing depth ratios from 0.05 to 1.2. At low depth ratios $\hat{d} < 0.3$, convection mainly occurs in the porous layer, Figs. 9(a) and (b). When

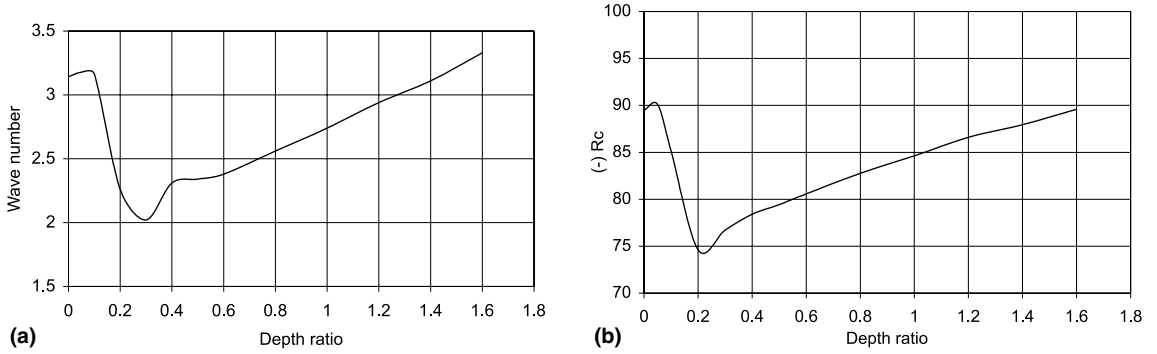

Fig. 8. Critical wave number and solutal Rayleigh number versus depth ratio for the salt-finger case.

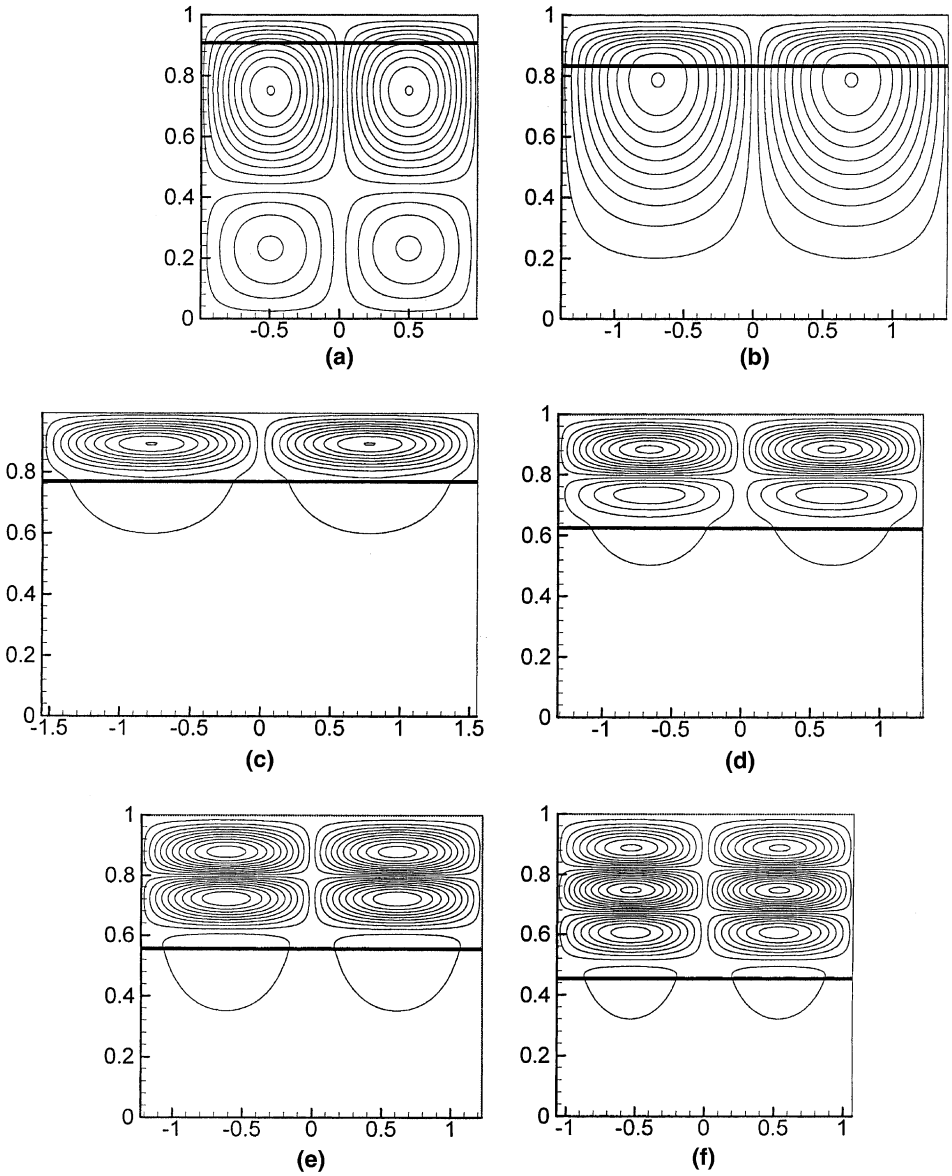

Fig. 9. Streamline patterns at the onset for the salt-finger case. The thick straight lines denote the liquid–porous interfaces. Depth ratios: (a) 0.1; (b) 0.2; (c) 0.3; (d) 0.6; (e) 0.8; (f) 1.2.

$\hat{d} = 0.3$, Fig. 9(c), convection is now confined within the fluid layer. As the depth ratio is increased further, the convection within the liquid layer becomes multi-cellular in the vertical direction. At $\hat{d} = 0.6$, Fig. 9(d), there are two cells in the vertical direction, which become fully developed at $\hat{d} = 0.8$, Fig. 9(e). When $\hat{d}$ reached 1.2, there are three fully developed convection cells in the liquid layer, Fig. 9(f). The vertical array of cells was also obtained by Chen and Chen [15]. However, their results show the instability of convective motion decreases sharply from the top to the lower cells whereas in our results, the changes are more gradual. Also in their results, the vertical array of convection cells appears at smaller depth ratios, for example, two-cell pattern appeared at $\hat{d} = 0.4$ in their case and at $\hat{d} = 0.6$ in our case.

For the salt-finger case, as in the thermal convection case, the general characteristics of the instability predicted by either the one-equation model or the two-equation model are quite similar. The difference in the critical values predicted by the two models is larger than those found for the thermal convection case.

Quantitative comparison between the two models for the salt-finger case is quite difficult. While both models used a same thermal Rayleigh number of 50 as one of the computational conditions, however, because of the conversion shown in Eq. (18), a constant R_a will result in different values of R_{a_m} or different values of $\hat{d}$, although R_a and R_{a_m} are logical parameters to keep constant in these two methods of calculation.

5. Conclusions

Stability analysis of double-diffusive convection in superposed fluid and porous layers has been carried out using a one-equation model. The results are compared with those obtained by using a two-equation model by Chen and Chen [15]. The major conclusions reached are:

1. For the thermal convection case, the bimodal nature of the marginal stability curve at low depth ratios, which was predicted by Chen and Chen [15], is also predicted by the one-equation model. The actual critical depth ratio values as predicted by the two models are slightly different.
2. The critical Rayleigh numbers for thermal convection as calculated by the one-equation model agree quite well with those predicted by the two-equation model of Chen and Chen [15]. The critical wave numbers as predicted by the one-equation model are lower than those predicted by the two-equation model.
3. For the salt-finger convection case, the general characteristics of the instability as predicted by the two models are similar. The differences in the predicted critical values are larger than those found in the thermal convection case.
4. Stability analysis carried out using the one-equation model is much less complicated than the two-equation model. The question which method yields the 'correct' values, i.e., critical Rayleigh number and wave number for a given depth ratio can only be answered by careful experimentation.
5. In all the above calculation cases, permeability is constant, but the present model can handle cases with arbitrarily distributed and anisotropical permeabilities which are very difficult for two-equation models to deal with.

References

[1] A.K. Sample, A. Hellawell, The mechanism of formation and prediction of channel segregation during alloy solidification, Metall. Trans. B 15 (1984) 2163–2173.
[2] C.F. Chen, F. Chen, Experimental study of directional solidification of aqueous ammonium chloride solution, J. Fluid Mech. 227 (1991) 567–586.
[3] S. Tait, C. Jaupart, Compositional convection in a reactive crystalline mush and melt differentiation, J. Geophys. Res. 97 (B5) (1992) 6735–6759.
[4] M.G. Worster, Instabilities of the liquid and mushy regions during solidification of alloys, J. Fluid Mech. 237 (1992) 649–669.
[5] F. Chen, J.W. Lu, T.L. Yang, Convection instability in ammonium chloride solution directionally solidified from below, J. Fluid Mech. 276 (1994) 163–187.
[6] D.M. Anderson, M.G. Worster, Weakly nonlinear analysis of convection in a mushy layer during the solidification of binary alloy, J. Fluid Mech. 302 (1995) 307–331.
[7] C.A. Chung, F. Chen, Onset of plume evolution in mushy layers, J. Fluid Mech. 408 (2000) 53–82.
[8] M.G. Worster, Convection in mushy layers, Annu. Rev. Fluid Mech. 29 (1997) 91–122.
[9] W.D. Bennon, F.P. Incropera, A continuum model for momentum, heat and species transport in binary solid–liquid phase change systems – I. Model formulation, Int. J. Heat Mass Transfer 30 (1987) 2161–2170.
[10] W.D. Bennon, F.P. Incropera, A continuum model for momentum, heat and species transport in binary solid–liquid phase change systems – II. Application to solidification in a rectangular cavity, Int. J. Heat Mass Transfer 30 (1987) 2171–2187.
[11] C. Beckermann, R. Viskanta, Natural convection solid/liquid phase change in porous media, Int. J. Heat Mass Transfer 31 (1988) 35–46.
[12] J.C. Heinrich, S. Felicelli, D.R. Poirier, Vertical solidification of dendritic binary alloys, Comput. Methods Appl. Mech. Eng. 89 (1991) 435–461.
[13] S.D. Felicelli, J.C. Heinrich, D.R. Poirier, Simulations of Freckles during vertical solidification of binary alloys, Metall. Trans. B 22 (1991) 847–859.
[14] P. Nandapurkar, D.R. Poirier, J.C. Heinrich, S. Felicelli, Thermosolutal convection during dendritic solidification of alloys: Part I. Linear stability analysis, Metall. Trans. B 20 (1989) 711–721.
[15] F. Chen, C.F. Chen, Onset of finger convection in a horizontal porous layer underlying a fluid layer, J. Heat Transfer 110 (1988) 403–409.
[16] S. Chandrasekhar, Hydrodynamic and Hydromagnetic Stability, Oxford University Press, Oxford 1961, pp. 34–43.
[17] E.R. Lapwood, Convection of a fluid in a porous media, Proc. Cambridge Philos. Soc. 44 (1948) 508–521.
[18] F. Chen, C.F. Chen, Experimental investigation of convective stability in a superposed fluid and porous layer when heated from below, J. Fluid Mech. 207 (1989) 311–321.
[19] F. Chen, C.F. Chen, Convection in superposed fluid and porous layers, J. Fluid Mech. 234 (1992) 97–119.